Received: 1 August 2022 | Revised: 11 September 2022 | Accepted: 13 September 2022

DOI: 10.1002/pol.20220434

RESEARCH ARTICLE

JOURNAL OF POLYMER SCIENCE WILEY

Multiscale rheology model for entangled Nylon 6 melts

Heyi Liang[1] | **Kenji Yoshimoto**[2] | **Masahiro Kitabata**[2] | **Umi Yamamoto**[2] | **Juan J. de Pablo**[1]

[1]Pritzker School of Molecular Engineering, The University of Chicago, Chicago, Illinois, USA

[2]Advanced Materials Research Laboratories, Toray Indurstires Inc., Otsu, Shiga, Japan

Correspondence
Kenji Yoshimoto, Toray Industries Inc., 3-2-1 Sonoyama, Otsu 520-0842, Japan.
Email: kenji.yoshimoto.z9@mail.toray

Juan J. de Pablo, Pritzker School of Molecular Engineering, The University of Chicago, Chicago, IL 60637, USA.
Email: depablo@uchicago.edu

Abstract

A multiscale simulation method is used to calculate the rheological properties of entangled Nylon 6 melts, including the stress relaxation modulus, storage and loss moduli, and the melt viscosity. The three-level multiscale approach includes all-atom, coarse-grained and slip-spring models, each operating at different levels of resolution and encompassing a wide range of length scales and over nine orders of magnitude in time. These models are unified by matching the polymer chain structure and dynamics as well as the stress relaxation, and together predict the rheological master curves at various temperatures using time–temperature superposition. The calculated viscosity agrees reasonably with experiment. The effect of polydispersity on rheology is also studied by simulating a polydisperse melt with chain lengths follow the Schulz-Zimm distribution. Under the same weight-average molecular weight, the polydisperse melt shows faster stress relaxation and lower viscosity compared to the monodisperse melt. For polymers that undergo rapid degradation at elevated temperatures, such as Nylon, the proposed approach offers a useful means to investigate rheology over a wide range of conditions. Importantly, the approach is fully predictive in that calculations of rheology are generated without relying on experimental information, and it therefore offers potential for design of polymeric materials on the basis of purely molecular models.

KEYWORDS

entanglement, multiscale simulations, polydispersity, polymer melts, viscoelastic properties

1 | INTRODUCTION

Nylon 6 is a versatile engineering plastic with excellent strength, toughness, heat resistance, and chemical resistance. Its industrial applications include automotive parts, electronics components, and fibers, many of which are manufactured by molding processes. During molding, Nylon 6 is heated to a temperature (T) above the melting point (T_m) to reduce the melt viscosity and increase the melt flow rate. The rheological properties of Nylon 6 melt depend not only on temperature, but also on the other processing conditions (e.g., shear stress and velocity) and the material characteristics (e.g., molecular weight, polydispersity, water absorption). Given the large number of the control variables, it is theoretically difficult to predict the rheological properties of Nylon 6.

A recent study of Nylon 6 has demonstrated the ability of the all-atom (AA) molecular dynamics (MD) simulations to predict the structural and relaxation characteristics in the melt state.[1] Although the system size of the MD simulations was relatively small, namely 27 chains of Nylon 6 with a degree of polymerization (DP) of 30, the resulting density, thermal expansion coefficient, static dielectric constant, and activation energy for the dielectric relaxation showed good agreement with experiment. The time scale of the simulations was limited to 100–200 ns due to the high computational demands associated with the AA model. To fully characterize the rheological properties of Nylon 6 melts, the simulation time scales must be extended to milliseconds or more.[2,3]

In this study, we build a bottom-up multiscale model to predict the rheological properties of Nylon 6 melts which links an all-atom (AA) model to a slip-spring (SS) model via a coarse-grained (CG) model.[3] For the AA model, we employ the same force field as that used in the abovementioned simulation study,[1] so that the effects of hydrogen bonding on the local structure and dynamics of Nylon 6 are taken into account. For the CG model, atoms from the AA model are grouped into CG beads by a graph-based method[4]; the force field is derived from the AA MD simulation results using the iterative Boltzmann inversion method.[5] The SS model adopted here have been described in prior publications.[6–8] Briefly, in the SS model, Nylon 6 molecules are mapped to bead-spring chains that reproduce the chain size in the CG model, where each bead represents multiple monomers. Artificial bonds between pairs of beads (i.e., slip-springs), which can slide along chains and be created/destroyed at chain ends, are introduced to represent entanglements between polymer chains. After proper renormalization of the time and modulus scales, we unify the three models to obtain a master curve that describes the linear viscoelasticity of the entangled Nylon 6 melt over 9 orders of magnitude in time. Since the multiscale simulations are performed at temperatures higher than experimental accessible range, time–temperature superposition is applied to extrapolate the rheological properties to experimentally accessible temperatures.

Polydispersity of polymers' molecular weight is an important factor that influence the linear viscoelasticity of entangled melts.[9–15] In commercial applications, Nylon 6 is usually synthesized from caprolactam by ring-opening polymerization with poor control over the molecular weight distribution, leading to large polydispersity. We extend our previous work[3] to polydisperse polymer samples, whose molecular weight is described by the Schulz-Zimm distribution, to study the effect of polydispersity on the rheology of Nylon 6 melts.

In what follows, we first describe the details of our bottom-up multiscale method for Nylon 6 melts (Models and Methods), and then characterize the structural and rheological properties using the simulation results (Results and Discussion). The resulting zero-shear viscosity of Nylon 6 melt is found to be in reasonable agreement with the experimental data, and the effect of polydispersity on linear viscoelasticity is studied, serving to illustrate the versatility of our bottom-up multiscale approach for prediction of the rheological properties of entangled polymer melts.

2 | MODELS AND METHODS

For the AA model, the optimized potential for liquid simulations (OPLS) were used to determine the force field parameters and partial charges.[16] The following partial charges were assigned on the atoms in the amide group: −0.50, 0.30, 0.50, and − 0.50 for the nitrogen (N), hydrogen (H), carbon (C), and oxygen (O) atoms, respectively. These values are similar to those used in a previous MD study of Nylon 6 melt[1] where the static and relaxational properties (e.g., density, activation energy for the dielectric relaxations) obtained from the simulations were shown to agree with the experimental data. In this study, AA MD simulations were performed using GROMACS.[17,18] The time step was set to 1 fs, and the linear constraint solver (LINCS) algorithm[19] was used to constrain the length of C–H bonds and to improve computational efficiency. An initial configuration was generated by randomly placing 100 chains of Nylon 6 (DP = 10, 20, 30, and 40) in a large simulation box (i.e., 0.1 g/cm^3). Also, initial velocities were assigned to all atoms, whose values were randomly generated from a Maxwell distribution at $T = 700$ K. This initial system was equilibrated with the following three steps. First, topological frustrations in the initial configuration were released by energy minimization using the steepest descent method. Then a short NVT simulation was performed to relax the initial chain conformations. Finally, an NPT simulation was performed over 10 ns under the ambient pressure (i.e., 1 atm) not only to relax the box size, but also to relax the polymer chains in a densely packed manner. The temperature and pressure were controlled with a Nose-Hoover thermostat and a Parrinello-Rahman barostat, respectively.[20] After the equilibration steps, NVT simulations were performed over 100 ns at $T = 700$ K to characterize the rheological properties of the Nylon 6 melts, where the thermodynamic properties (e.g., temperature, pressure tensor) and the atom positions were sampled at every 1 and 10 ps, respectively. To estimate the shifting factors for the time–temperature superposition, the same equilibration steps and production run were conducted at several different temperatures ($T = 500$, 600, 900, and 1100 K).

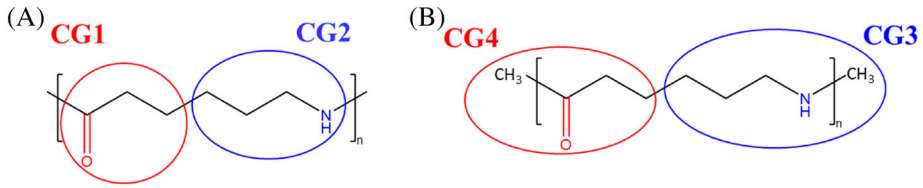

FIGURE 1 Coarse-grained representation of Nylon 6 for (A) repeat units, and (B) chain ends.

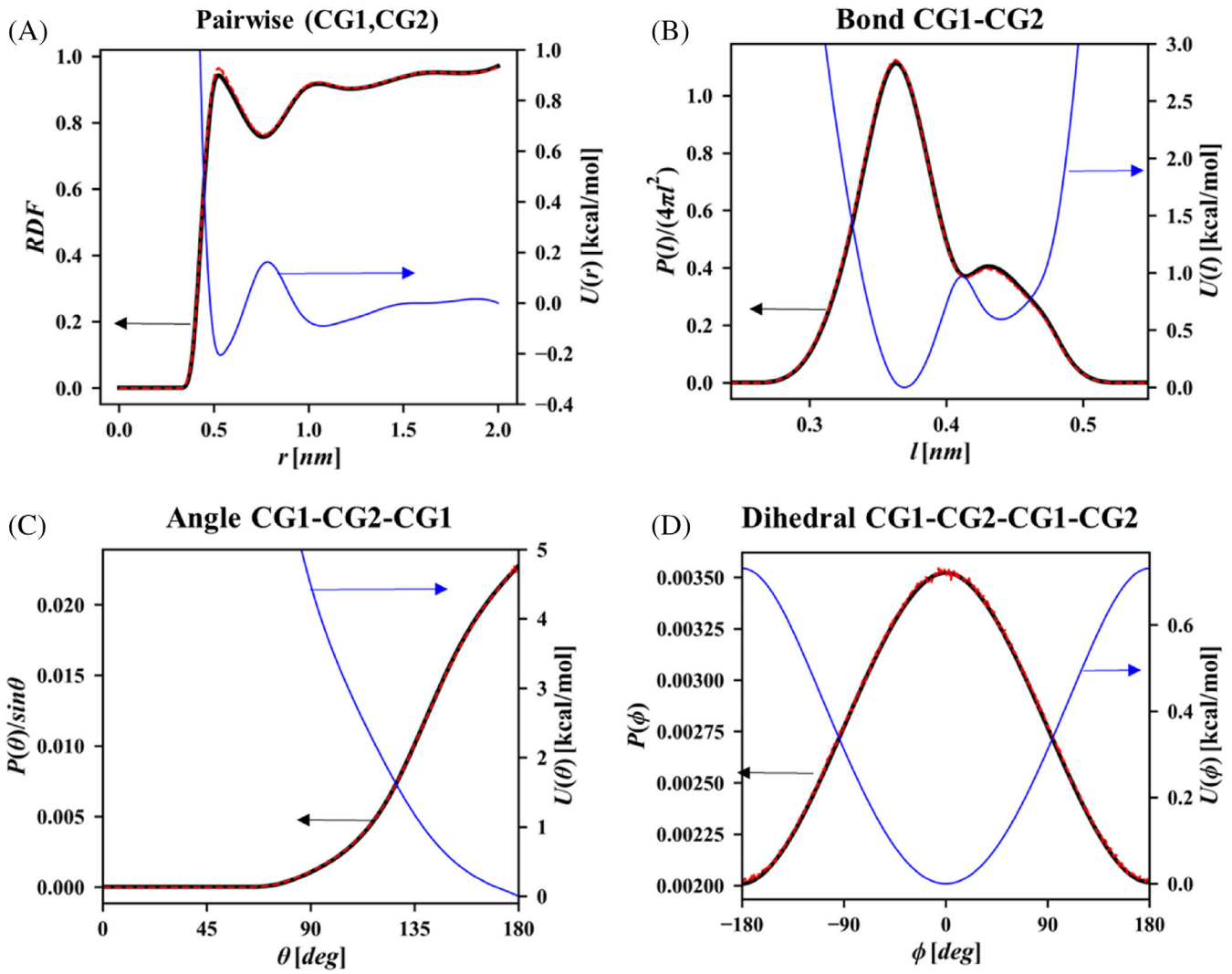

FIGURE 2 Representative coarse-grained force field and distribution functions of (A) pairwise, (B) bond, (C) angle, and (D) dihedral interactions. Black solid lines and red dashed lines are distribution functions from reference all-atom (AA) simulations and from coarse-grained (CG) simulations, respectively. Blue solid lines are CG potentials.

To build a CG model, the CG representation of Nylon 6 was first determined by the graph-based coarse-graining method (GBCG).[4] In this method, a molecule is regarded as a graph where atoms are mapped onto nodes and bonds are edges that connect them. CG representations with lower resolutions can be obtained by iteratively grouping nodes and performing edge contractions. In our CG model, a caprolactam monomer (i.e., a repeat unit) was mapped to two CG beads with different bead types as shown in Figure 1A. Since each Nylon 6 chain was capped with a CH3 group on each end, we treated the chain ends differently and assigned different CG bead types to them (Figure 1B). The CG force fields for this model was derived using the iterative Boltzmann inversion (IBI) method, where the CG potential was updated iteratively to minimize the difference between the distribution function (e.g., radial, bond length, bond angle and dihedral angle distribution functions) from CG and AA models. To derive the CG force field, we used the AA simulation of the Nylon 6 melt with DP = 40 as the

reference, and Figure 2 shows the representative CG non-bonded, bonded, angle and dihedral potentials as well as the corresponding distribution functions in CG and AA models. CG simulations of Nylon 6 melts with degrees of polymerization DP = 10 ~ 100 were then performed at 700 K. The melts were first relaxed in the NPT ensemble at 1 atm, using a Nose-Hoover style thermostat and barostat. Then a production run was carried out to calculate the density, chain structure, primitive path (only for DP = 100), chain dynamics and stress relaxation modulus. The integration timestep was set to $\Delta t = 3$ fs. All CG simulations are performed by LAMMPS.[21]

A model with even lower resolution, that is, the SS model, was then parameterized to speed up the simulation of highly entangled Nylon 6. In this model, polymers are modeled by the bead-spring chains, where beads interact with each other through a soft repulsive potential. The connectivity between bonded beads is provided by harmonic springs. Each bead can represent over tens of monomers, giving rise to a very soft potential between beads. This further leads to bond-crossing and unphysical disentanglement dynamics. In order to preserve entanglements, artificial bonds, called "slip-springs", are introduced between pairs of beads belonging to different polymer chains. The Hamiltonian of the SS model can be written as

$$\mathcal{H} = \mathcal{H}_{nb} + \mathcal{H}_{b} + \mathcal{H}_{ss} \tag{1}$$

$$\beta\mathcal{H}_{nb} = \sqrt{\overline{N}} \int \frac{d\boldsymbol{r}}{R_{ee}^3} \frac{\kappa N}{2} \phi^2(\boldsymbol{r}) \tag{2}$$

$$\beta\mathcal{H}_{b} = \frac{3}{2} \sum\nolimits_i \frac{r_{b_i}^2}{b^2} \tag{3}$$

$$\beta\mathcal{H}_{ss} = \frac{3}{2} \sum\nolimits_i \frac{r_{ss_i}^2}{b_{ss}^2} \tag{4}$$

Equation (2) describes the Hamiltonian of the non-bonded potential, which depends on the inverse compressibility κ, the local bead density $\phi(\boldsymbol{r})$, and the invariant degree of polymerization $\overline{N} = \left(\rho_{ss} R_{ee}^3 / N\right)^2$, where ρ_{ss} is the bead number density, R_{ee} is the end-to-end distance of the polymer chain, N is the number of beads in each chain. Equations (3) and (4) are the Hamiltonians of the bonded and SS potentials, where r_{b_i} and r_{ss_i} are lengths of the i-th bond and the i-th SS, b^2 and b_{ss}^2 are the mean squared bond lengths of bonds and SSs. $\beta = 1/(k_B T)$, where k_B is the Boltzmann constant and T is the absolute temperature. The configuration of the system is updated by a hybrid MD/MC method, where the positions of beads are evolved by molecular dynamics (MD) using the Brownian dynamics equation of motion, and the SSs are updated through Monte-Carlo (MC) moves every $\tau_{ss} = 1$ MD steps. The SSs can hop along a chain and be created/destroyed at chain ends, mimicking chain reptation and constraint release, respectively. The number of SSs can fluctuate and is controlled by a fugacity $z = \exp(\mu/k_B T)$ in the grand canonical ensemble, where $k_B T$ is the thermal energy and μ is the pseudo-chemical potential of SSs. Details of the MC moves can be found in our previous publications.[7,8] In our SS simulations, each bead represents 5 monomers, so an entangled strand is modeled by $N_{e,ss} = 3$ beads. The bead number density is determined by $\rho_{ss} = \rho R_{ee}^3 N_{e,ss} N_A / (M_0 N_e)$, where N_A is the Avogadro constant, $M_0 = 113.16$ g/mol is the molar mass of the monomer, $\rho = 0.877$ g/cm^3 is the density, $R_{ee} = 1.082(\mathrm{DP})^{0.5}$ nm is the end-to-end chain distance, $N_e = 15$ is the degree of polymerization (DP) of an entangled strand. The latter three parameters (i.e., ρ, R_{ee} and N_e) are obtained from CG simulations at 700 K. The SS simulations were performed in reduced units, with length unit $\sigma = R_e$, energy unit $\epsilon = k_B T$, and mass unit m (which is the mass of each bead). The integration timestep of the MD move was set to $\Delta t = 0.0002\tau_{MD}$, where $\tau_{MD} = (m\sigma^2/\epsilon)^{1/2}$.The prediction of polymer melt rheology relies on calculation of the stress relaxation modulus, $G(t)$, which is obtained by the Green-Kubo relation

$$G(t) = \frac{V}{k_B T} \left\langle \sigma_{\alpha\beta}(t_0 + t) \sigma_{\alpha\beta}(t_0) \right\rangle_{t_0, \alpha\beta} \tag{5}$$

where V is the volume of the simulation box, $\sigma_{\alpha\beta}(t)$ represent the off-diagonal components of the stress tensor, and the bracket $\langle ... \rangle_{t_0,\alpha\beta}$ denotes the average over all possible t_0 as well as the average of three off-diagonal components of the stress tensor ($\alpha\beta = xy, yz, xz$). To compare the simulation results to experiment, the stress relaxation modulus is first fitted with a generalized Maxwell model (Equation 6) and then converted to the storage and loss moduli, $G'(f)$ and $G''(f)$, using Fourier transforms (Equations 7 and 8)

$$G(t) = \sum\nolimits_p G_p \exp\left(-\frac{t}{\tau_p}\right) \tag{6}$$

$$G'(f) = \sum\nolimits_p \frac{G_p \left(2\pi f \tau_p\right)^2}{1 + \left(2\pi f \tau_p\right)^2} \tag{7}$$

$$G''(f) = \sum\nolimits_p \frac{G_p 2\pi f \tau_p}{1 + \left(2\pi f \tau_p\right)^2} \tag{8}$$

where G_p and τ_p are the modulus and relaxation time of the p-th mode, and f is the frequency.

Note that in our previous work,[3] we focused on the polystyrene (PS) melts to prove concept of the bottom-up multiscale approach. Unlike PS, Nylon 6 forms hydrogen bonds between the polymer chains via the amide groups (–CONH–), which may affect the structural and dynamic properties of the Nylon 6 melt. It is therefore uncertain whether the same approach can be applied to the Nylon 6 melt. It has been predicted theoretically[22] and observed in many experiments[23,24] that associative interactions (such as hydrogen bonds) between polymer chains can drastically change the melt rheology. However, at high temperatures, the lifetime of hydrogen bonds is too short to affect the rheological properties of polymers. For example, Karimi-Varzaneh et al[25] have shown by all-atom simulations that the relaxation of the hydrogen bond network dominates the dynamics of the Nylon 6,6 melt only at low temperatures ($T < 413$ K). They have also shown[26] that the coarse-grained model of Nylon 6,6, which is lack of explicit hydrogen bond description, can reproduce the dynamics of the atomistic model at high temperatures ($T > 500$ K) with simple renormalization of coarse-grained timescale. Considering the chemical structure similarity between Nylon 6,6 and Nylon 6, we would expect that the simple coarse-grained force field derived by the iterative Boltzmann inversion method is capable of describing the Nylon 6 dynamics at temperatures $T > 500$ K.

3 | RESULTS AND DISCUSSION

3.1 | Validation of the coarse-grained model

The coarse-grained (CG) model is parameterized from the all-atom (AA) model, so a good CG model should reproduce important physical properties of its parent AA model. To validate the CG model, we compare the melt density, chain structure, chain dynamics as well as the stress relaxation modulus between the CG and the AA models. We also analyze the primitive path of long Nylon 6 melts and compare the entanglement molecular weight to experimental results.

3.1.1 | Density

Figure 3A compares the density of Nylon 6 melts with different DPs obtained from both AA and CG simulations. In both simulations, the melt density increases with increasing DP and saturates at large DPs. This can be justified by the fact that chain ends have larger free volume than other repeat units at the chain center. Such chain end effect can also be quantified by

$$\frac{1}{\rho}=\frac{1}{\rho_\infty}+\frac{C}{DP} \tag{9}$$

where ρ_∞ is the density at infinite chain length and C is a numerical coefficient that depends on the chemical structure of repeat units and chain ends. Figure 3B shows the relation between $1/\rho$ and $1/DP$. The comparison of density shows that the CG model reproduces the density from the AA model with the best accuracy at DP = 40. This is because the CG force fields are derived based on the AA model with DP = 40. However, the CG model underestimates the density by 4% for the lowest DP and overestimates by 1% at infinite DP. The lack of chain end CG beads in the melt leads to insufficient sampling of their partial radial distribution functions, leading to inaccurate CG non-bonded potentials. The deviations between the CG and AA density are therefore larger at low DP, where there are more chain ends, and smaller at high DP.

3.1.2 | Chain structure

To characterize the chain structure, we calculate the mean squared internal distance, $\langle R^2(n)\rangle$, which is the mean squared distance between two backbone CG beads separated by n CG bonds. In order to compare the AA model results to those of the CG model, we convert the AA configuration to the CG one using the CG representation as shown in Figure 1. Figure 4A shows the comparison of the mean squared internal distance of Nylon 6 chain with DP = 40 obtained from both AA and CG models. In both models, the Nylon 6 chain adopts a rod-like conformation at small length scales for short chain segments with $n < 3$, as shown by the $\langle R^2(n)\rangle \propto n^2$ power law; then it assumes an ideal conformation at larger length scales for longer chain segments with $n > 30$, as indicated by the $\langle R^2(n)\rangle \propto n$ scaling relation. The good quantitative agreement between the two models shows that the CG model is able to reproduce the chain structure observed in the AA model.

We can also estimate the chain stiffness by plotting the mean squared end-to-end distance $\langle R_{ee}^2\rangle$ predicted by the CG model as a function of the molecular weight, as shown in Figure 4B. The mean squared chain size increases linearly with molecular weight when $M > 4000$ g/mol, as illustrated by the linear fit (red dashed line) $\langle R_{ee}^2\rangle = 0.01026M$ nm^{2}mol/g. Using the fitting result together with the method provided by Wu,[27] the characteristic ratio of Nylon 6 is obtained as $C_\infty = 6.6$, which is only 6% higher than the experimental measurement $C_{\infty,expr} = 6.2$. It is important to predict the precise chain stiffness using the CG model since the

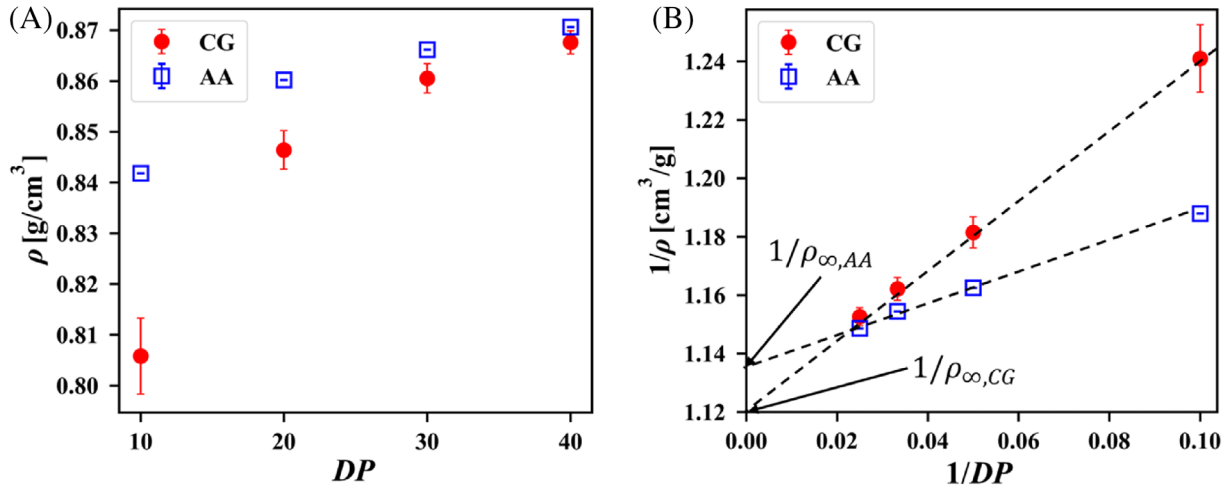

FIGURE 3 Density of Nylon 6 melts with different degree of polymerization. (A) Density versus degree of polymerization. (B) Inverse density versus inverse degree of polymerization. Dashed lines are best linear fit.

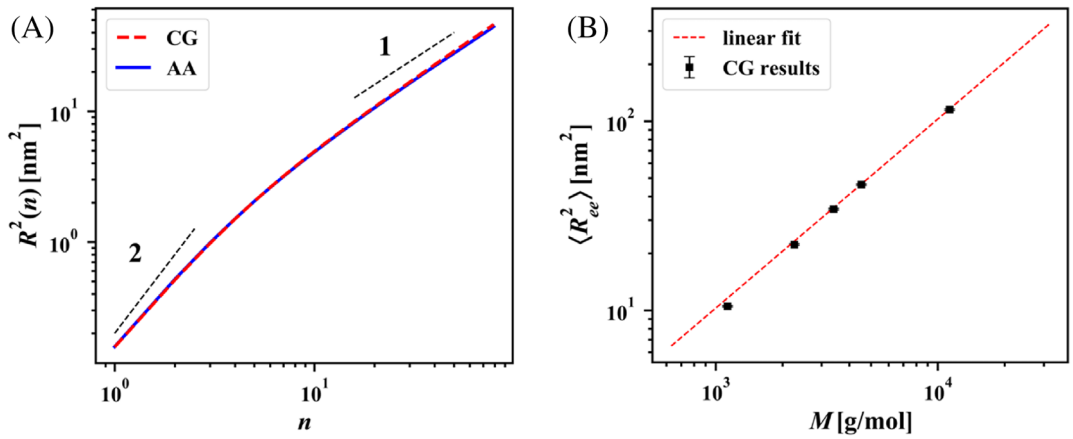

FIGURE 4 (A) Comparison of the mean squared internal distance of Nylon 6 chains with degree of polymerization, DP = 40, between all-atom (AA, blue solid line) and coarse-grained (CG, red dashed line) simulations. (B) Mean squared end-to-end distance of Nylon 6 chains with different molecular weight obtained from CG simulations. The red dashed line is the best linear fit, $\langle R_{ee}^2 \rangle = 0.01026\,M\ \mathrm{nm^2\,mol/g}$, demonstrating the ideal chain conformation in the melt.

entanglements in polymer melts are related to it, as discussed in the next sub-section.

3.1.3 | Entanglement molecular weight

The entanglement molecular weight in long polymer melts is determined by the melt density and chain stiffness, which are both predicted reasonably well by the CG model as shown in previous sub-sections. Therefore, it is expected that the CG model can also predict the entanglement molecular weight. To calculate it, we analyze the primitive path of the CG Nylon 6 melt with DP = 100 using the Z1 algorithm.[28–30] The entanglement degree of polymerization obtained from the primitive path analysis is $N_e = 15$, which corresponds to an entanglement molecular weight $M_e \cong 1700\,\mathrm{g/mol}$. Compared to the experimental value[31] $M_{e,\mathrm{expr}} \cong 2000\,\mathrm{g/mol}$, the CG model predicts lower entanglement molecular weight by 15%. This is due to the overestimation of the chain stiffness in the CG model. Fetters et al[31] have shown that the entanglement molecular weight is related to the characteristic ratio by the following scaling relation

$$M_e \propto \langle R_{ee}^2 \rangle^{-3} \propto C_\infty^{-3} \tag{10}$$

According to Equation (10), if the chain stiffness is overestimated by 6%, the entanglement molecular weight will be underestimated by $1-(1/1.06)^3 \cong 16\%$, which agrees with our observation. This error analysis demonstrates that a good CG model with high accuracy in chain stiffness is crucial for the reliable prediction of melt entanglements.

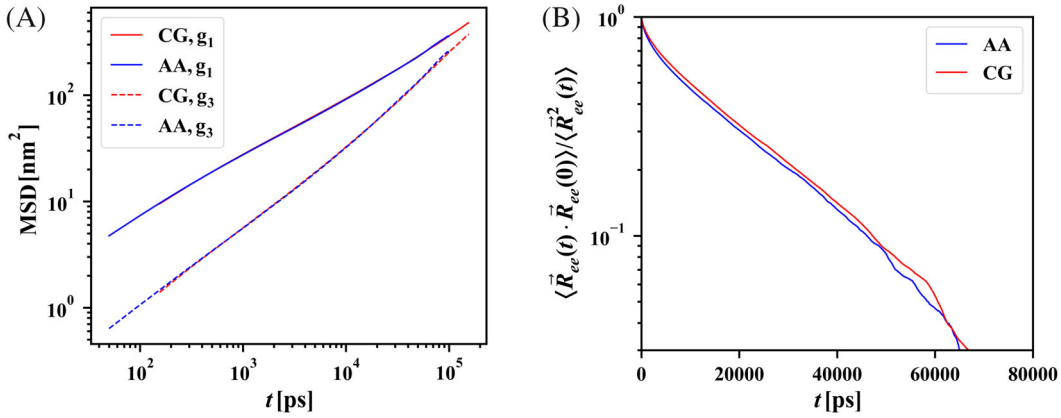

FIGURE 5 Comparing (A) the mean squared displacement (MSD) of monomers (g_1, solid lines) and chains (g_3, dashed lines), and (B) the autocorrelation function of the chain end-to-end vector between all-atom (AA, blue) and coarse-grained (CG, red) simulations of Nylon 6 with degree of polymerization DP = 30. The time of the CG simulation is renormalized by $\tau_{CG-AA} = 5.64$.

3.1.4 | Chain dynamics

During coarse-graining, the degrees of freedom in a system are reduced, leading to smoother local energy barriers for monomer diffusion in the CG model. In order to predict the correct dynamics, the timescale of the CG model must be renormalized according to $t = \tau_{CG-AA} \times t_{CG}$, where t is the renormalized time, t_{CG} is the actual time in the CG model, and τ_{CG-AA} is the time renormalization factor that accounts for the change in the local friction. To obtain the time renormalization factor, we compare the translational and orientational relaxation of chains. The translational relaxation can be described by the mean squared displacement (MSD) of the monomers, g_1, and center of mass of chains, g_3, while the orientational relaxation can be characterized by the autocorrelation function of the chain end-to-end vector, $\langle \boldsymbol{R_{ee}}(t) \cdot \boldsymbol{R_{ee}}(0) \rangle / \langle \boldsymbol{R_{ee}^2}(t) \rangle$. Figure 5 shows the translational and orientational relaxation analyzed for the Nylon 6 melt with DP = 30, from both the AA and CG models. The timescale of the CG model is renormalized by $\tau_{CG-AA} = 5.64$. Since the CG model does not have atomic resolution, it is expected that the CG results deviate at very short timescales when atomistic details dominate the relaxation. At longer timescales, the CG model can faithfully reproduce the dynamics of the AA model after time renormalization.

3.1.5 | Stress relaxation modulus

The linear viscoelastic response of a polymer melt can be fully characterized by the stress relaxation modulus, $G(t)$. Figure 6 shows $G(t)$ for the Nylon 6 melt with DP = 30, which compares the results obtained from the AA and CG models. The noise of $G(t)$ at long time from the CG model is due to the stress fluctuation around 0 when the melt is fully relaxed and can be suppressed by running simulations with much larger boxes. In order to account for the local dynamic speed-up, the timescale of the CG model is renormalized by $\tau_{CG-AA} = 5.64$, as discussed in the previous sub-section. Note that for melts with shorter chains, in order to match the AA and CG stress relaxation modulus, the renormalization of the CG modulus by a modulus renormalization factor, γ_{CG-AA}, is necessary due to a mismatch of the AA and CG melt densities. However, for long chains, such as DP = 30 and 40, the CG model reproduces the AA melt density and the renormalization of CG modulus is not necessary, that is, $\gamma_{CG-AA} = 1$.

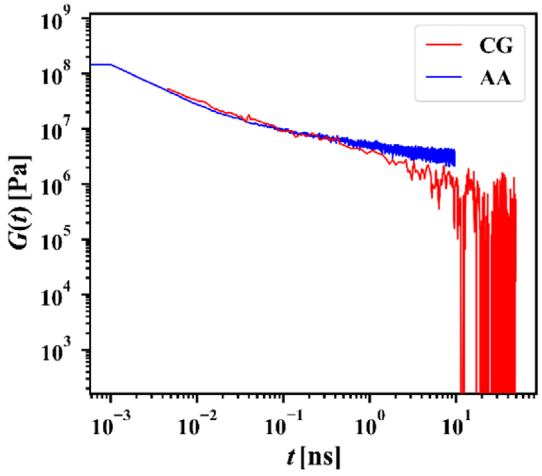

FIGURE 6 Comparing the stress relaxation modulus between all-atom (AA, blue) and coarse-grained (CG, red) simulations of Nylon 6 with degree of polymerization DP = 30. The time of the CG simulation is renormalized by $\tau_{CG-AA} = 5.64$. The modulus of the CG simulation is renormalized by $\gamma_{CG-AA} = 1$.

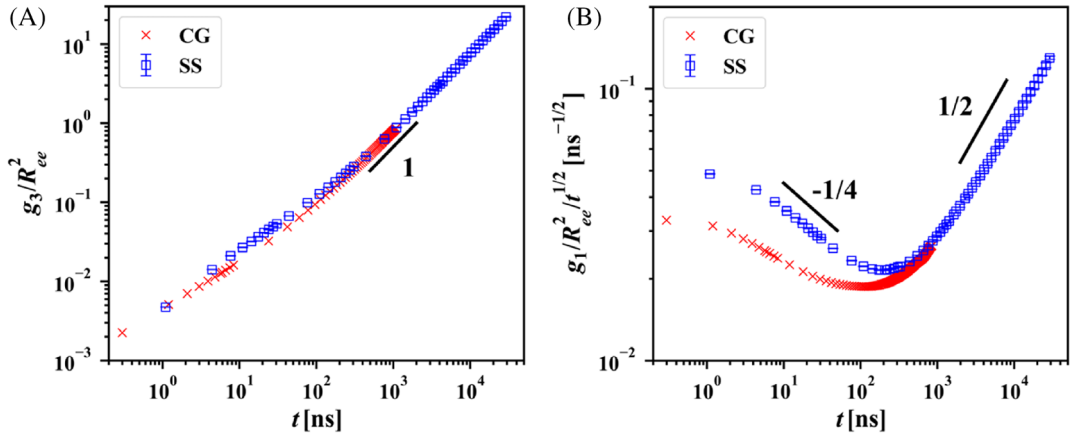

FIGURE 7 Comparison of (A) normalized chain mean-squared displacement and (B) normalized monomer mean-squared displacement between coarse-grained (CG, red cross) and slip-spring (SS, blue squares) simulations of Nylon 6 with degree of polymerization DP = 100. The time scale of the SS simulation is renormalized by $\tau_{SS-CG} = 55\,\text{ns}/\tau_{MD}$. Error bars of the SS data are obtained from six independent samples.

3.2 | Validation of the slip-spring model

The SS model is a phenomenological model that describes the dynamics of entangled polymer melts. The SS model of Nylon 6 is parameterized by the CG model of entangled Nylon 6 melts and its ability to reproduce the entanglement dynamics is investigated in this section.

3.2.1 | Chain dynamics

The translational relaxation of chains in the Nylon 6 melt with DP = 100 is characterized by the MSD of the monomers, g_1, and center of mass of chains, g_3, for both CG and SS models. Note that, in this context, a "monomer" in the SS model is a bead that represents a chain segment consisting of 5 caprolactam repeat units. The configuration of the CG model is also converted by grouping each 10 CG beads into a larger SS bead since each caprolactam repeat unit is modeled by two CG beads. All MSD values are normalized by the mean squared chain size, R_{ee}^2, so the MSD becomes dimensionless and can be compared between models having different resolutions. The timescale of the SS model is renormalized by a time renormalization factor $\tau_{SS-CG} = 55\,\text{ns}/\tau_{MD}$, where τ_{MD} is the time unit of the SS model. This factor is obtained by minimizing the difference of normalized chain MSD in the diffusive regime, where $g_3/R_{ee}^2 \sim t$, between the CG and SS models, as shown in Figure 7A. For entangled polymer melts, the MSD of monomers/segments shows a distinct scaling regime that depends on the relaxation time, t. At relatively short relaxation times ($t < \tau_e$, where τ_e is the entanglement time), the relaxation of strands between entanglements is described by Rouse dynamics with a scaling relation $g_1 \sim t^{1/2}$. In the chain reptation regime ($\tau_e < t < \tau_R$, where τ_R is the Rouse time), strands relax through Rouse-like diffusion along the primitive path with a scaling relation $g_1 \sim t^{1/4}$. After the Rouse time ($\tau_R < t < \tau_{rep}$, where τ_{rep} is the reptation time), all monomers in the chain move coherently, and the whole chain diffuses along the primitive path which leads $g_1 \sim t^{1/2}$. Finally, after the reptation time ($\tau_{rep} < t$), the whole chain diffuses along the entire primitive path and is fully relaxed, and the monomer MSD enters the diffusive regime, $g_1 \sim t$. In order to identify these scaling regimes and distinguish different scaling exponents, we normalize g_1 by $t^{1/2}$. Figure 7B compares the normalized segmental MSD, $g_1/R_{ee}^2/t^{1/2}$, between the CG and SS models. Both models show a decrease of the normalized MSD with a slope $-1/4$, corresponding to the chain reptation regime. Note that while the SS model captures the long-time behavior of the CG model, its relaxation is faster at shorter timescales when $t < 2 \times 10^2$ ns. The orientational relaxation of polymer chains in the Nylon 6 melt with DP = 100 is characterized by the autocorrelation function of the chain end-to-end vector, $\langle \boldsymbol{R_{ee}}(t) \cdot \boldsymbol{R_{ee}}(0) \rangle / \langle \boldsymbol{R_{ee}^2}(t) \rangle$. Figure 8 compares the orientational relaxation of chains between the CG and SS models. The time of the SS model is renormalized by $\tau_{SS-CG} = 55\,\text{ns}/\tau_{MD}$ as obtained from the g_3 analysis. There is good agreement between the CG and SS models. Although the translational relaxation of chain segments in the SS model is faster than that of the CG model, the orientational relaxation of the whole chain matches that of the CG mode very well.

3.2.2 | Stress relaxation modulus

Figure 9 compares the stress relaxation modulus, $G(t)$, of the Nylon 6 melt with DP = 100 between the CG and SS models. The time scale for the SS model is renormalized by $\tau_{SS-CG} = 55\,\text{ns}/\tau_{MD}$ as mentioned above. Since the SS

model uses a different Hamiltonian to describe the entangled melt, it is also necessary to renormalize its modulus, that is, elastic energy per unit volume, so its value can match that of the CG model. The results after multiplying $G(t)$ of the SS model by a modulus renormalization factor, γ_{SS-CG}, are shown in Figure 9A. The value of the renormalization factor is $\gamma_{SS-CG} = 8.0 \times 10^6\ \mathrm{Pa}/G_0$, where $G_0 = \rho_{ss} k_B T$. At short time scales, the stress relaxation modulus of the SS model deviates from that of the CG model. This is expected because the spatial resolution of the SS model is 5 repeat units per bead and relaxation modes of chain segments on that or smaller length scales are absent in the model, leading to the observed deviation at shorter times. To demonstrate the entanglement characteristics of the entangled Nylon 6 melt, we also normalize the stress relaxation moduli of both models by $t^{1/2}$ as shown in Figure 9B. For an entangled melt, the relaxation at short length scales follows the Rouse model so the stress relaxation modulus changes as $G(t) \sim t^{-1/2}$, which leads to a constant plateau in Figure 9B. At time scales longer than the entanglement time, τ_e, the stress relaxation slows down and eventually flattens to form an entanglement plateau at G_e. Although there is no apparent plateau in Figure 9A due to the relatively short chains (less than 10 entanglements per chain), lines with positive slopes in Figure 9B still demonstrate much slower dynamics compared to Rouse as a result of chain entanglements. This is followed by the entanglement regime and the terminal relaxation regime, where the stress exponentially decays to zero. SS simulations with longer chains exhibit a clear entanglement plateau (see later sections), but the CG simulations are limited to chains of intermediate length by the computational demands associated with large system size and long relaxation time. Given these restrictions, the good agreement of the stress relaxation in the entanglement regime for the moderately entangled melt is a manifestation of the success of the SS model in capturing the entanglement dynamics of the CG model.

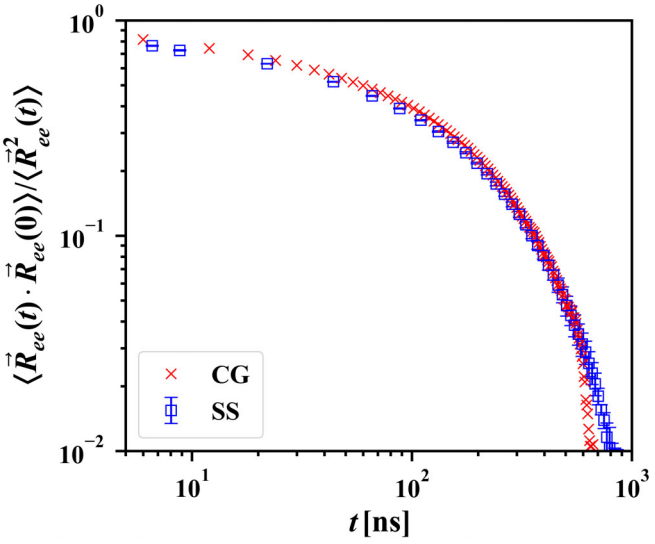

FIGURE 8 Comparison of the chain end-to-end autocorrelation function between coarse-grained (CG, red cross) and slip-spring (SS, blue squares) simulations of Nylon 6 with degree of polymerization DP = 100. The time scale of the SS simulation is renormalized by $\tau_{SS-CG} = 55\ \mathrm{ns}/\tau_{MD}$. Error bars of the SS data are obtained from six independent samples.

3.3 | Time–temperature superposition

To facilitate the chain relaxation in both AA and CG models, the simulation temperature is set at 700 K, which

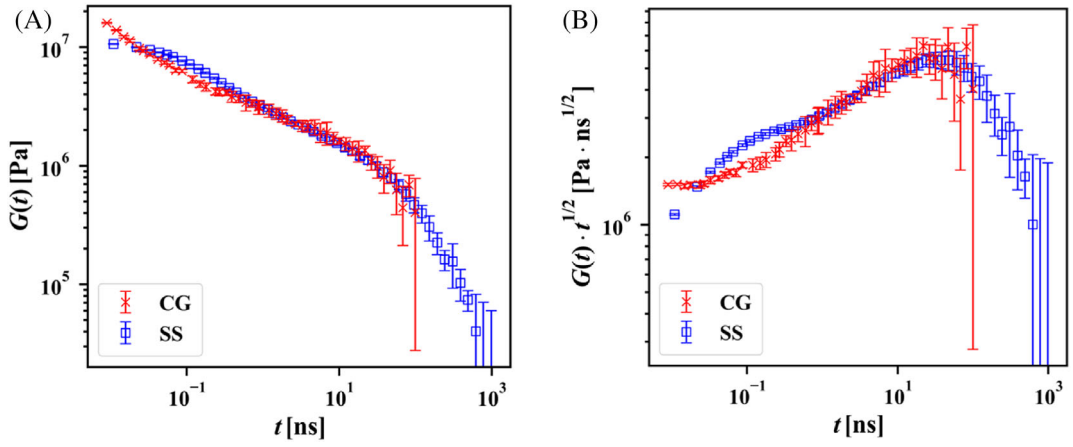

FIGURE 9 Comparison of (A) stress relaxation modulus and (B) normalized stress relaxation modulus between coarse-grained (CG, red cross) and slip-spring (SS, blue squares) simulations of Nylon 6 with degree of polymerization DP = 100. The time and modulus scales of the SS simulation are renormalized by $\tau_{SS-CG} = 55\ \mathrm{ns}/\tau_{MD}$ and $\gamma_{SS-CG} = 8.0 \times 10^6\ \mathrm{Pa}/G_0$, respectively. Error bars of the CG and SS data are obtained from three and six independent samples, respectively.

is much higher than the experimental accessible range (usually below 600 K). To compare simulation results to experiments, we apply the time–temperature superposition to simulation data. Following routine experimental practice, we perform simulations of the AA model at different temperatures from 500 to 1100 K and calculate the stress relaxation modulus $G(t)$ using Equation (5). As shown in Figure 10A, $G(t)$ calculated at different temperatures are first vertically shifted by the modulus scale shift factor, b_T, which is obtained by

$$b_T = \frac{\rho(T)T}{\rho_0 T_0} \tag{11}$$

where $\rho(T)$ and ρ_0 are densities at temperature T and reference temperature T_0, respectively. $\rho(T)/(kg/m^3) = 1309.9 - 0.631 \times \mathrm{T/K}$ is measured from simulations and we choose $T_0 = 500K$. Then we shift the time scale by a factor a_T, which is obtained as the horizontal shift factor that minimizes the difference of $G(t)$ for different temperatures. Figure 10A shows the procedure of time–temperature superposition applied to Nylon 6 melts with DP = 40. Figure 10B summarizes a_T for different DPs and best fits (dashed lines) to the WLF equation:

$$a_T = \exp\left[-\frac{c_1(T - T_0)}{c_2 + T - T_0}\right] \tag{12}$$

It is observed that while a_T depends on chain size, it saturates for long chains (DP = 30 and 40). We therefore apply the a_T obtained from the melt with DP = 40 to melts of longer chains, with $c_1 = 4.7944$, $c_2 = 430.521$ K.

3.4 | Multiscale master curves

Polymer melts with molecular weight much higher than the entanglement molecular weight, $M_w \gg M_e$, share similar stress relaxation moduli at time scales shorter than the entanglement time. The differences show up as different lengths of the entanglement plateau, that is, different reptation times. To predict the full spectrum stress relaxation modulus, that is, the master curve $G(t)$, of highly entangled polymer melts with different molecular weights, one only need to run simulations of the SS model with different DPs to capture the molecular weight dependent disentanglement behavior. The stress relaxation at shorter times can be obtained from the AA model of low molecular weight melts and the CG model of slightly entangled melts. In our approach, the master curve is obtained by combining results from three models of decreasing resolution but increasing time and length scales (see Figure 11A). The short time stress relaxation modulus that characterizes the relaxation of chain segments containing a few monomers is obtained from the AA model of melts with DP = 40. At larger length scales and longer time scales when the relaxation is limited to chain segments shorter than or comparable to an entangled segment, the stress relaxation is calculated by the CG model of melts with DP = 100 and 200. For the longest relaxation and longer chains where entanglements dominate the relaxation, the SS model is used to predict the stress relaxation for polymers with various DPs from 100 to 400 (i.e., from 7 to 27 entanglements per chain). To calculate the master curve, the CG $G(t)$ is time-shifted by $\tau_{CG-AA} = 5.38$, and the SS $G(t)$ is both time-shifted by

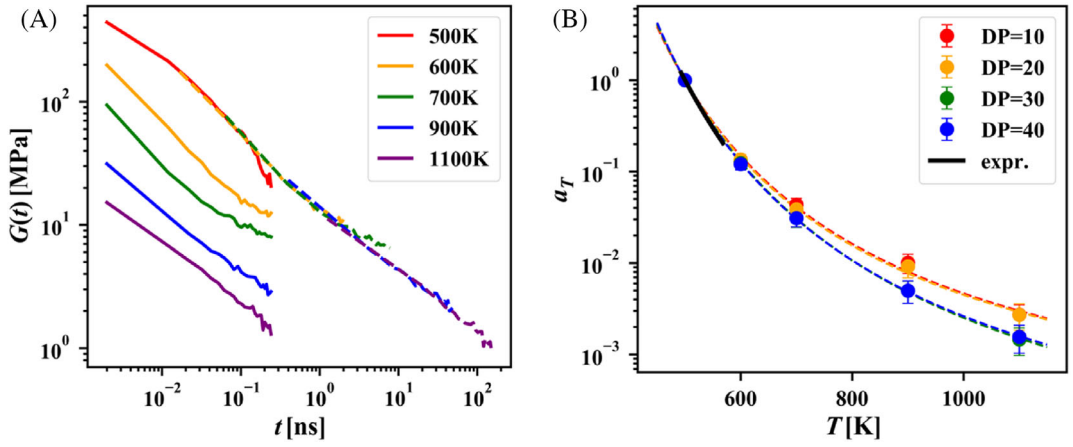

FIGURE 10 (A) Stress relaxation modulus, $G(t)$, of Nylon 6 melts with degree of polymerization DP = 40 obtained from all-atom simulations at $T = 500 \sim 1100$ K. Solid and dashed lines are stress relaxation modulus before and after shifting, respectively. (B) Time shift factor, a_T, as a function of temperature for Nylon 6 melts with different degrees of polymerization. Dashed lines are best fits to Equation (12). The black line is the experimental time shift factor determined between 220 and 295°C by the Arrhenius equation $\ln a_T = E_a/R(1/T - 1/T_0)$, where the activation energy is $E_a = 55$ kJ/mol and R is the gas constant.

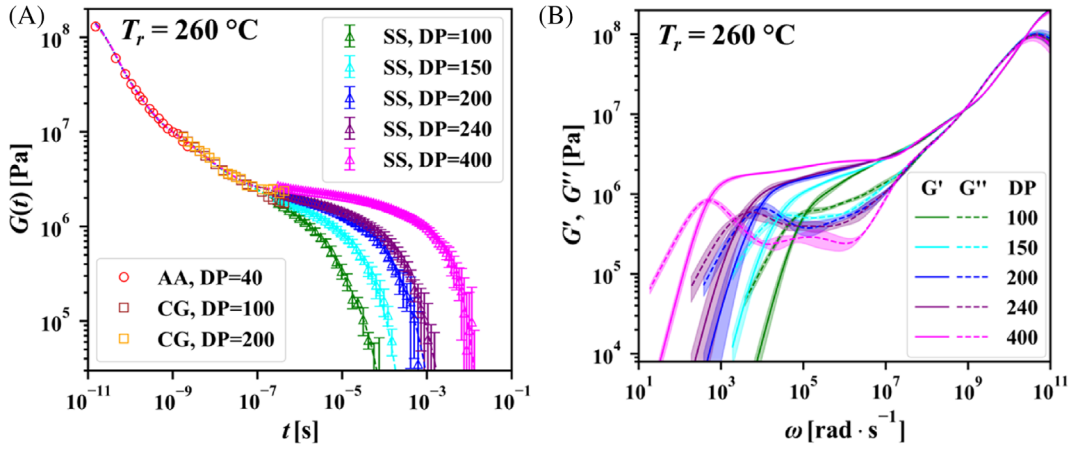

FIGURE 11 (A) Stress relaxation modulus, $G(t)$, of Nylon 6 melts with degree of polymerization DP = 100 ~ 400. Dashed lines represent best fits with the generalized Maxwell model (Equation 6). Error bars are obtained from six independent samples. (B) Storage (G', solid lines) and loss (G'', dashed lines) moduli of Nylon 6 melts with DP = 100 ~ 400. Both storage and loss moduli are calculated from the fitting results of the stress relaxation modulus using Equations (7) and (8). The shaded area represents the uncertainty obtained from six independent samples. All data are shifted to the reference temperature $T_r = 260°C$.

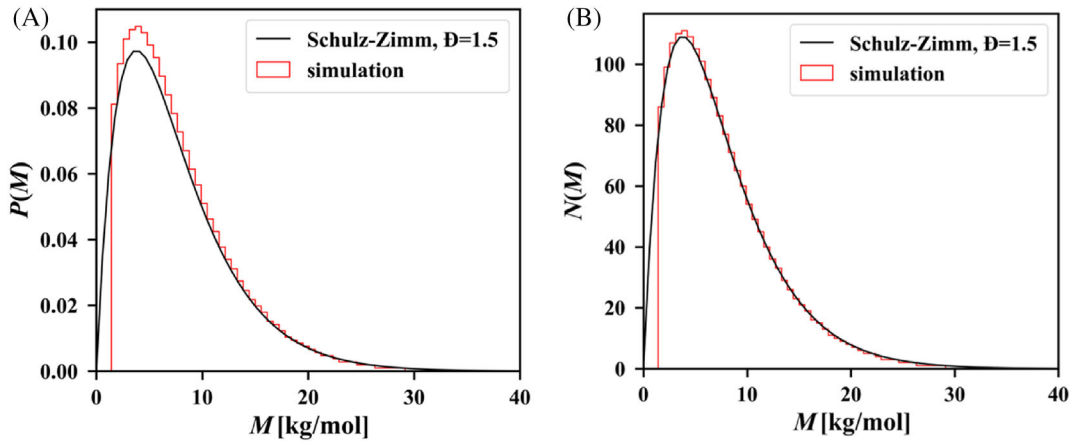

FIGURE 12 (A) Number fraction, $P(M)$, and (B) number, $N(M)$, of Nylon 6 chains with different molecular weight, M. Black curves are Schulz–Zimm distribution (Equation 13) with polydispersity Đ = 1.5 and weight-average molecular weight $M_w = 11.3$ kg/mol. Red histograms are molecular weight distribution of the polydisperse Nylon 6 melt in the slip-spring simulation.

$\tau_{SS-AA} = \tau_{SS-CG} \times \tau_{CG-AA} = 295.9\,\text{ns}/\tau_{MD}$ and modulus-shifted by $\gamma_{SS-AA} = \gamma_{SS-CG} \times \gamma_{CG-AA} = 8.0 \times 10^6\,\text{Pa}/G_0$ ($\gamma_{CG-AA} = 1$), while the AA $G(t)$ is taken as the "ground truth" and is not changed. Master curves of Nylon 6 melts with different DPs are fitted with the generalized Maxwell model using 12 modes (Equation 6) and converted to storage and loss moduli (Equations 7 and 8), as shown in Figure 11B. Both the stress relaxation modulus and storage and loss moduli are shifted to the reference temperature $T_r = 260°C$ using the time–temperature superposition method described in the previous section. The viscosities of melts are also calculated and will be discussed in Section 3.6.

3.5 | Effect of polydispersity

Nylon 6 can be synthesized by ring-opening polymerization of caprolactam, and the molecular weight of the product can be described by the Schulz-Zimm distribution,[32]

$$P(M) = \frac{z^{z+1}}{\Gamma(z+1)} \frac{M^{z-1}}{M_n^z} \exp\left(\frac{-zM}{M_n}\right) \tag{13}$$

where $P(M)$ is the number fraction of polymer chains with molecular weight M, M_n is the number-average

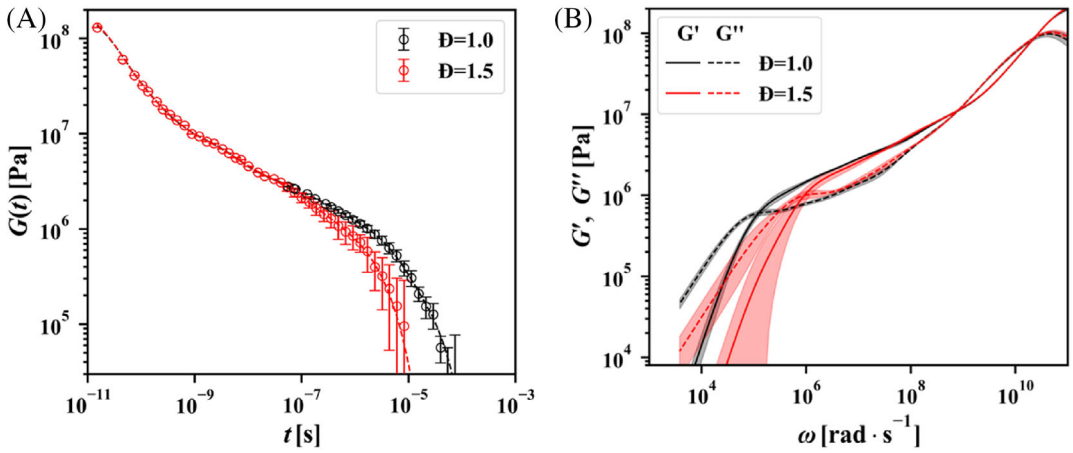

FIGURE 13 (A) Stress relaxation modulus, $G(t)$, of monodisperse (black) and polydisperse (red) Nylon 6 melts with the same weight-average molecular weight, $M_w = 11.3\,\text{kg/mol}$. Dashed lines are best fits to the generalized Maxwell model (Equation 6). Error bars are obtained from six independent samples. (B) Storage (G', solid lines) and loss (G'', dashed lines) moduli Nylon 6 melts in panel (A). Both storage and loss moduli are calculated from the fitting results of the stress relaxation modulus using Equations (7) and (8). Shadow area represent uncertainty obtained from six independent samples. All data are shifted to the reference temperature $T_r = 260°C$.

molecular weight, $\Gamma(z+1)$ is the Gamma function, and z is related to the polydispersity index $Đ = M_w/M_n = (z+1)/z$ in which M_w is the weight-average molecular weight. We modeled a polydisperse Nylon 6 melt with $Đ = 1.5$ using the SS model and its molecular weight distribution is shown in Figure 12. Note that in the SS simulation, we remove chains shorter than the entanglement strand since they are not expected to contribute to the reptation dynamics, and their volume fraction is also very low (<1%).

Figure 13 compares the rheology of monodisperse and polydisperse Nylon 6 melts with the same weight-average molecular weight, $M_w = 11.3\,\text{kg/mol}$, which corresponds to DP = 100. The polydisperse melt shows faster stress relaxation (see Figure 13A). This phenomenon is consistent with what Peters et al[14,15] have observed from CG simulations of polydisperse polyethylene melts. The faster stress relaxation also leads to a shorter entangled regime and earlier disentangled time (see Figure 13B). In the polydisperse sample, the slow dynamics of long chains has prominent contribution to $G(t)$ at long time but is not sufficiently sampled due to the scarcity of them (see Figure 12B). This leads to large variations of $G(t)$ at long time. The zero-shear viscosity of melts can be calculated by integrating the stress relaxation modulus

$$\eta = \int_0^\infty G(t)\mathrm{d}t = \sum\nolimits_p G_p \tau_p \tag{14}$$

where the second equality is obtained by Equation (6). At $T_r = 260\,°C$, the zero-shear viscosity of the polydisperse melt $\eta(Đ = 1.5) = 3.1 \pm 1.5\,\text{Pa}\cdot\text{s}$ is lower than that of the monodisperse melt $\eta(Đ = 1.0) = 11.9 \pm 1.5\,\text{Pa}\cdot\text{s}$.

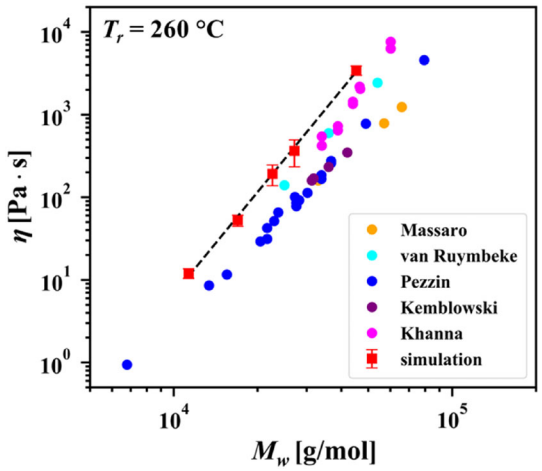

FIGURE 14 Dependence of the Nylon 6 melt viscosity on the weight-average molecular weight from both simulations and experiments. All data are shifted to the reference temperature $T_r = 260°C$. Simulation results are obtained from monodisperse melts. The black dashed line is the best fit to Equation 15.

3.6 | Comparison to experimental measurements

In Figure 14, we show the dependence of the melt viscosity of Nylon 6 on the weight-average molecular weight predicted by the multiscale simulation method, and compare it to experimental measurements.[33–37] All simulation results are obtained by Equation (14) and shifted to $T_r = 260\,°C$ according to the time–temperature superposition procedure described in the previous section. All experimental results are also shifted to $T_r = 260\,°C$ using

the time shift factor calculated by $\ln a_T = E_a/R(1/T - 1/T_0)$, where the activation energy is $E_a = 55\,\mathrm{kJ/mol}$ for temperatures in the range of $220 \sim 295°\mathrm{C}$ and R is the gas constant.[34,36] Note that the viscosity obtained by Pezzin et al[33] is reported in terms of the number-average molecular weight, so we estimate the weight-average molecular weight by assuming a polydisperse index of 2, which is a common value for polymers synthesized through condensation. The molecular weight dependence of the simulation viscosity can be described by the scaling law

$$\eta \propto (M/M_e)^{\alpha} \tag{15}$$

where the scaling power is $\alpha = 3.9 \pm 0.1$. Such scaling power is slightly higher than 3.4 as predicted by the reptation theory, but has been reported from experiments of entangled 1,4-polyisoprene melts.[38] The simulated viscosities are slightly above the experimental ones from Khanna et al.[35] and from van Ruymbeke et al.[37] They are also above those of Pezzin et al.,[33] Kemblowzki et al.[34] and Massaro et al.[36] We attribute the discrepancies to three effects. First, the CG model underestimates the entanglement molecular weight by approximately 15%, which leads to overestimation of the viscosity by a factor of $0.85^{-\alpha} = 1.9$. Second, Nylon 6 is not stable and can degrade at high temperatures with trace amounts of water content.[33,34,39] The experimental viscosity measured at high temperatures might therefore correspond to smaller molecular weights than those reported. Third, the chain degradation might lead to a large polydispersity and therefore results in a lower viscosity, as demonstrated in the previous section.

4 | CONCLUSIONS

A multiscale simulation method has been used to predict the rheological properties of entangled Nylon 6 melts, including the stress relaxation modulus, storage and loss moduli, as well as the melt viscosity. The three-level multiscale simulation adopted here includes all-atom, coarse-grained and SS models, each operating at different levels of resolutions that enable access to larger length and longer time scales. The rheological properties are passed from a high-resolution model to a low-resolution model by matching the chain conformation, the translational and rotational relaxation behavior of chains as well as the stress relaxation of melts. We also study the effect of polydispersity on linear viscoelasticity by comparison between a monodisperse melt and a polydisperse melt characterized by the Schulz-Zimm molecular weight distribution. Long chains relax faster in the polydisperse melt due to faster relaxation of constraints posed by shorter chains, leading to a faster stress relaxation and a lower viscosity. The model is fully predictive in that the rheological behavior over time scales spanning nine orders of magnitude can be estimated solely on the basis of an atomistic model, without recourse to adjustable parameters or experimental data. For Nylon 6, the agreement with measured viscosities is shown to be very reasonable, serving to validate the usefulness of the overall approach for situations in which the rheology is not known or is difficult to measure experimentally, as is the case with polymeric materials that degrade easily at elevated temperatures, which limits the use of time–temperature superposition techniques.

ACKNOWLEDGMENTS

Computation time was partially provided by Research Computing Center, The University of Chicago. Partial support from NIST through the Center for Hierarchical Materials Design (CHiMaD) is gratefully acknowledged.

CONFLICT OF INTEREST

The authors declare no conflicts of interest.

ORCID

Heyi Liang https://orcid.org/0000-0002-8308-3547
Kenji Yoshimoto https://orcid.org/0000-0003-0097-4297
Masahiro Kitabata https://orcid.org/0000-0002-6656-7128
Juan J. de Pablo https://orcid.org/0000-0002-3526-516X

REFERENCES

[1] N. V. Lukasheva, D. A. Tolmachev, V. M. Nazarychev, J. M. Kenny, S. V. Lyulin, *Soft Matter* **2017**, *13*, 474.
[2] A. F. Behbahani, L. Schneider, A. Rissanou, A. Chazirakis, P. Bačová, P. K. Jana, W. Li, M. Doxastakis, P. Polińska, C. Burkhart, M. Müller, V. A. Harmandaris, *Macromolecules* **2021**, *54*, 2740.
[3] H. Liang, K. Yoshimoto, P. Gil, M. Kitabata, U. Yamamoto, J. J. de Pablo, *Macromolecules* **2022**, *55*, 3159.
[4] M. A. Webb, J.-Y. Delannoy, J. J. de Pablo, *J. Chem. Theory Comput.* **2019**, *15*, 1199.
[5] D. Reith, M. Pütz, F. Müller-Plathe, *J. Comput. Chem.* **2003**, *24*, 1624.
[6] A. Ramírez-Hernández, M. Müller, J. J. D. Pablo, *Soft Matter* **2013**, *9*, 2030.
[7] A. Ramírez-Hernández, B. L. Peters, M. Andreev, J. D. Schieber, J. J. de Pablo, *J. Chem. Phys.* **2015**, *143*, 243147.
[8] A. Ramírez-Hernández, B. L. Peters, L. Schneider, M. Andreev, J. D. Schieber, M. Müller, J. J. de Pablo, *J. Chem. Phys.* **2017**, *146*, 014903.
[9] M. Rubinstein, R. H. Colby, *J. Chem. Phys.* **1988**, *89*, 5291.
[10] C. Tsenoglou, *Macromolecules* **1991**, *24*, 1762.
[11] S. H. Wasserman, W. W. Graessley, *J. Rheol.* **1992**, *36*, 543.

[12] P. Cassagnau, J. P. Montfort, G. Marin, P. Monge, *Rheol. Acta* **1993**, *32*, 156.
[13] D. Nichetti, I. Manas-Zloczower, *J. Rheol.* **1998**, *42*, 951.
[14] B. L. Peters, K. M. Salerno, T. Ge, D. Perahia, G. S. Grest, *Phys. Rev. Lett.* **2018**, *121*, 057802.
[15] B. L. Peters, K. M. Salerno, T. Ge, D. Perahia, G. S. Grest, *Macromolecules* **2020**, *53*, 8400.
[16] W. L. Jorgensen, D. S. Maxwell, J. Tirado-Rives, *J. Am. Chem. Soc.* **1996**, *118*, 11225.
[17] H. J. C. Berendsen, D. van der Spoel, R. van Drunen, *Comput. Phys. Commun.* **1995**, *91*, 43.
[18] D. Van Der Spoel, E. Lindahl, B. Hess, G. Groenhof, A. E. Mark, H. J. C. Berendsen, *J. Comput. Chem.* **2005**, *26*, 1701.
[19] B. Hess, H. Bekker, H. J. C. Berendsen, J. G. E. M. Fraaije, *J. Comput. Chem.* **1997**, *18*, 1463.
[20] D. Frenkel, B. Smit, *Understanding Molecular Simulation: From Algorithms to Applications*, Elsevier, San Diego, CA **2001**.
[21] S. Plimpton, *J. Comput. Phys.* **1995**, *117*, 1.
[22] M. Rubinstein, A. N. Semenov, *Macromolecules* **1998**, *31*, 1386.
[23] A. Shabbir, H. Goldansaz, O. Hassager, E. van Ruymbeke, N. J. Alvarez, *Macromolecules* **2015**, *48*, 5988.
[24] C. L. Lewis, K. Stewart, M. Anthamatten, *Macromolecules* **2014**, *47*, 729.
[25] H. A. Karimi-Varzaneh, P. Carbone, F. Müller-Plathe, *Macromolecules* **2008**, *41*, 7211.
[26] H. A. Karimi-Varzaneh, P. Carbone, F. Müller-Plathe, *J. Chem. Phys.* **2008**, *129*, 154904.
[27] S. Wu, *Polym. Int.* **1992**, *29*, 229.
[28] M. Kröger, *Comput. Phys. Commun.* **2005**, *168*, 209.
[29] N. C. Karayiannis, M. Kröger, *Int. J. Mol. Sci.* **2009**, *10*, 5054.
[30] R. S. Hoy, K. Foteinopoulou, M. Kröger, *Phys. Rev. E* **2009**, *80*, 031803.
[31] L. J. Fetters, D. J. Lohse, D. Richter, T. A. Witten, A. Zirkel, *Macromolecules* **1994**, *27*, 4639.
[32] P. C. Hiemenz, T. P. Lodge, *Polymer Chemistry*, CRC Press, Boca Raton, FL **2007**.
[33] G. Pezzin, G. B. Gechele, *J. Appl. Polym. Sci.* **1964**, *8*, 2195.
[34] Z. Kembłowski, J. Torzecki, *Rheol. Acta* **1983**, *22*, 186.
[35] Y. P. Khanna, P. K. Han, E. D. Day, *Polym. Eng. Sci.* **1996**, *36*, 1745.
[36] R. Massaro, P. Roozemond, M. D'Haese, P. V. Puyvelde, *Int. Polym. Process.* **2018**, *33*, 327.
[37] E. van Ruymbeke, J. J. M. Slot, M. Kapnistos, P. A. M. Steeman, *Soft Matter* **2013**, *9*, 6921.
[38] M. Abdel-Goad, W. Pyckhout-Hintzen, S. Kahle, J. Allgaier, D. Richter, L. J. Fetters, *Macromolecules* **2004**, *37*, 8135.
[39] D. J. Dijkstra, *Pure Appl. Chem.* **2009**, *81*, 339.

How to cite this article: H. Liang, K. Yoshimoto, M. Kitabata, U. Yamamoto, J. J. de Pablo, *J. Polym. Sci.* **2022**, *60*(22), 3071. https://doi.org/10.1002/pol.20220434